JOURNAL of ELECTROCHEMICAL SCIENCE and TECHNOLOGY

RESEARCH ARTICLE

Ligand Stripped Vanadium Trifluoride Nanocrystals with Churros Structure as Novel Anode Material in Lithium Ion Batteries

Youngmin Chi[1†] | Jaekwang Kim[1†] | Hyunchul Kang[2] | Minki O[1] | Hwasuk Nam[1] Taejong Paik[1]* | Songhun Yoon[1]*

[1]Department of Nanomaterials Science & Engineering, School of Integrative Engineering, Chung-Ang University, Heuksukro 84, Dongjakgu, Seoul, Korea

[2]Se2Materials, 14, Gyoyuk-gil, Naju-si, Jeollanam-do, Republic of Korea

[†]These authors contributed equally to this work

CORRESPONDENCE
T: +82-2-820-5769
F: +82-2-814-2651
E: paiktae@cau.ac.kr (T. Paik), yoonshun@cau.ac.kr (S. Yoon)

https://doi.org/10.33961/jecst.2024.00927

VOLUME 16 ISSUE 2 MAY 2025

ABSTRACT

Herein, the churros-like nanocrystal of vanadium trifluoride (VF_3) is prepared using a high temperature nanoparticle synthesis method and applied into the anode material in lithium ion batteries. A novel shape nanostructure is firstly observed from our synthesis and the surface ligand is stripped in order to obtain clean surface, which can reduce the irreversible decomposition in anode application. When applied into anode as conversion-based charge storage, a high discharge capacity of 607 mAh g^{-1} at 0.1 C rate, which is the highest value in the reported VF_3 anode materials. Also, a gradual increase of discharge capacity into 633 mAh g^{-1} at the 500th cycle under 0.2 C rate is observed, which is attributed to the typical conversion reaction mechanism of our materials. From galvanostatic charge-discharge patterns and electrochemical impedance spectroscopy, it is observed that very limited increase in overall resistance is observed even after 500 cycles. These highly advanced anode performances of our churros like VF_3 nanocrystals is ascribed to a high accessible lithium ion and well-dispersed nanocrystal morphology in maintaining nanocrystal shape after long-term charge-discharge.

KEYWORDS

Churros shape, Nanocrystal, VF_3, Anode, Conversion reaction

RECEIVED 02 September 2024 **ACCEPTED** 21 October 2024

OPEN ACCESS This is an open-access article distributed under the terms of the Creative Commons Attribution Non-Commercial License (http://creativecommons.org/licenses/by-nc/4.0) which permits unrestricted non-commercial use, distribution, and reproduction in any medium, provided the original work is properly cited.

INTRODUCTION

There has been a continuous requirement of developing electrode materials with high energy and power density for Li-ion secondary batteries (LIBs) because of growing demands of high capacity applications, for instance, electric vehicles (EV), hybrid electric vehicles (HEVs), plug-in electric vehicles (PHEVs) and energy storage system (ESS) [1–4]. However, a conventional anode material, graphite already has a capacity limit due to its theoretical capacity (372 mAh g^{-1}), which strongly drives researchers to explore substitutable materials. As one of the candidates of graphite anode materials, conversion reaction based materials become a clue to satisfaction of the high-energy density since these materials have several merits such as low cost, easy preparation and high capacity. Nano-structurization of these materials has exhibited a possibility to surpass common limitation issues, such as slow kinetic properties and large volumetric changes accompanying with bond breakage and metal formation. As one of the typical nanocrystal preparation methods, colloidal synthesis, the pure bottom-up approach via molecular precursors, has been intensively studied because it can provide delicate control of composition, crystal shape and size, which can be beneficial to find the solution to overcome the mentioned limitations [5–9]. In spite of recent advance in nanostructured and conversion-based materials on LIBs [10,11], the preparation and electrochemical studies about metal fluorides (MFs) have rarely been conducted as anode materials application in LIBs. It is reported that MFs undergo electrochemical reaction with Li-ion (Li^+) (and its reverse reaction) as follows:

$MF_n + nLi^+ + ne^- \leftrightarrow M/LiF$ (Here, n is the formal oxidation state of metal and e is electron)

Also, it has been well-known that LiF known as a poor electronic and ionic conductor at ambient temperature has a high bond dissociation energy from high electronegativity difference, and electrochemical activity can occur in the form of M/LiF composites where amorphous M/LiF are mixed on an atomic or a nanometer scale [12,13]. Among several MF series, Vanadium trifluoride (VF_3) can be considered as a promising anode material since it can carry three electrons during conversion reaction showing a high theoretical capacity of 745 mAh g^{-1}. Although its maximum capacity is much higher than that of the graphite, there have hardly been reported on VF_3 that shows reasonable reversibility and stability to the best of our knowledge. Here, we report VF_3 nanocrystals with churros-like novel structure VF_3 which is prepared by facile colloidal synthesis and following ligand stripping method for adaptation of surface ligand. After morphological and structural analysis, novel VF_3 nanocrystals are applied into anode material using conventional slurry mixing electrode coating. The VF_3 nanocrystals were prepared via solution phase synthesis, which is reported for the first time. The VF_3 nanocrystals are highly dispersed in nonpolar solvent and easily deposited on various types of substrates via room-temperature solution-based preparation, which allows facile and rapid preparation in electrochemical electrodes.

EXPERIMENTAL

Synthesis of VF_3 Nanocrystals (VF_3 NCs)

1-Octadecene (60 mL, ©Sigma aldrich), oleic acid (3.2 mL, ©Sigma aldrich), oleylamine (20 mL, ©Sigma aldrich) and vanadium oxyfluoride (VOF_3, 0.5 g, ©Alfa aesar) were added to a 250 mL three-neck flask. While stirring, the flask was degassed at 105°C for 2 h. Reaction mixture in the flask was heated to 300°C (ramping rate: 10°C min^{-1}) in nitrogen (99.999 mol/mol%) atmosphere. For growth of nanocrystals, temperature was remained for 30 min. After the crystal growth, reaction vessel was cooled down to ambient temperature. Refinement was done by centrifugation (6000 RPM, 2 min) after addition of n-hexane and excess amount of ethanol. Residue was dispersed in 10 ml of n-hexane.

Ligand stripping of VF_3 Nanocrystals (VF_3 LSNCs)

5 mL of the VF_3/n-hexane sol was transferred to a conical tube. Appropriate amount of triethyloxoborofluorate (Et_3OBF_4, ©Alfa aesar) was dispersed in 2 mL of N,N-dimethylformamide (DMF, ©Sigma aldrich). The Et_3OBF_4 solution was poured onto the VF_3/n-hexane sol and vortexed for 5 min. Purification was conducted by excess toluene/n-hexane (1:1 (v/v%)) sol. Precipitate was dried in vacuum oven at 40°C overnight. Remaining

powder was collected and stored in vacuum desiccator [14].

Material Characterization

Morphological information was characterized by field emission scanning electron spectroscope (FE-SEM, SIGMA, Carl Zeiss) and transmission electron microscope (TEM, JEOL, JEM-ARM200F). X-ray diffraction spectroscopy (XRD, Bruker-AXS, New D8-Advance) was utilized to verify crystal structure of the prepared material. Fourier-transform infrared (FT-IR) spectra were obtained by Thermo Scientific Nicolet 6700 spectrometer.

Electrochemical Analyses

2032 type coin cells were constructed to analyze Li^+ battery performance of VF_3. Three types (commercial bulk, NC and LSNC material) of VF_3 powder (80 wt%) was first mixed with carbon black (10 wt%) in an agate mortar (The bulk VF_3 material was purchased from ©Alfa aesar). Then PVDF (10 wt%) binder and NMP (N-Methyl-2-pyrrolidone) were added and mixed until homogeneous slurry obtained. The slurry was coated onto Cu foil and the coated foil was dried in convection oven at 80°C for 30 min. The dried foil was punched to get 11 mm disks. Mass-loading was from 1.25 to 1.27 mg per single current collector. The prepared disks then dried in vacuum oven overnight at 80°C to evaporate NMP thoroughly. 140 μL of 1.0 M $LiPF_6$ in ethylene carbonate (EC):ethyl methyl carbonate (EMC) (3:7 (v/v%)) electrolyte was used during cell construction in Ar filled glove box (H_2O < 1 ppm).

Lithium metal was utilized as the anode in the half-cell configuration. Galvanostatic charge-discharge (0.02–2.8 V vs. Li/Li^+) and electrochemical impedance spectroscopy (EIS) was conducted on the prepared cells by ©Wonatech WBC 3000 battery cycler and Iviumstat (Ivium technology) respectively. The EIS was conducted at 0.02–2.8 V vs. Li/Li^+ at the middle of charge and discharge (constant current of 0.5 C was applied).

RESULTS AND DISCUSSION

Morphological investigation of the as-prepared material was conducted by SEM and TEM. Fig. 1a shows SEM image of as-prepared VF_3 material, which exhibited nano-sized churros like nano particles (Diameter: 30–60 nm, height ~60 nm). To our best knowledge, we successfully prepared VF_3 nanocrystal with churros like

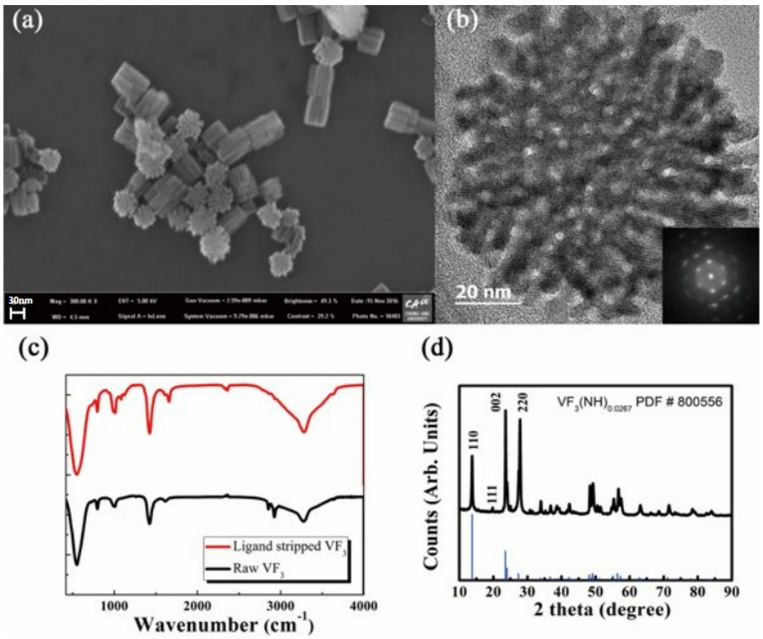

Fig. 1. (a) SEM and (b) TEM image of VF_3 nanocrystal. (c) FT-IR spectra of NC (black) and LSNC (red). (d) XRD spectra of VF_3 LSNC.

shape for the first time. As can be seen TEM image in Fig. 1b, it seems that the particle comprises a bundle of nanorods with vacant site. However, note that each particle proved to be a single crystalline by the Fast Fourier Transformation (FFT) of TEM results (inset of Fig. 1b). Therefore, it is certain that churros VF_3 consists of interconnected nanorods that include vacant space between them. Fig. 1c shows FT-IR spectra of the churros VF_3 before and after ligand stripping by Meerwein's salt, Et_3OBF_4. Attenuated intensity of C–H stretching modes (2800–3000 cm^{-1}) of a salt treated sample confirmed the clear removal of ligands came from organic capping agents [15,16]. Subsequently, XRD spectra of the ligand removed sample was obtained in Fig. 1d and confirm the highly crystalline VF_3 with minute trace of amine (JCPDS PDF-01-080-0556). VF_3 crystallizes in the hexagonal $P6_3/mmc$ space group, with unit cell parameters of a = 5.27 Å and c = 6.35 Å, as determined by X-ray diffraction analysis. In this structure, V atoms occupy octahedral sites coordinated by six F atoms, forming a layered configuration. The average V–F bond length is approximately 2.0 Å, which contributes to the compound's structural stability and influences its electrochemical properties as an anode material. Typically, surface ligands such as oleic acids can retard the access of electrolyte because of surface protection effect of nanocrystals. Hence, the ligand stripping using Et_3OBF_4 can be helpful in charging-discharging due to its clean surface without further electrochemical decomposition of ligand itself. In addition, it is well-known that conversion reaction as anode application has accompanied a large volume change during charging-discharging. It is predictable that these vacant sites within churros VF_3 can provide a space for mechanical relaxation during conversion reaction.

The electrochemical behavior of VF_3 anodes were investigated through galvanostatic charge/discharge (Fig. 2). Each bulk, NC and LSNC represents a commercially purchased bulk VF_3, the prepared VF_3 nanocrystal and ligand stripped VF_3 nanocrystal, respectively. Fig. 2 shows charge (lithiation, voltage decreases) and discharge (delithiation, voltage increases) profiles of the individual anodes at initial, 50^{th}, 200^{th} and 400^{th} cycle, which were obtained at 0.1 C rate (current density: 74.5 mA g^{-1}) and voltage window of 0–2.8 V (vs. Li/Li^+). Each profile of bulk, NC and LSNC anodes revealed that 1^{st} cycle delivered charge/discharge capacity of 860/485, 983/

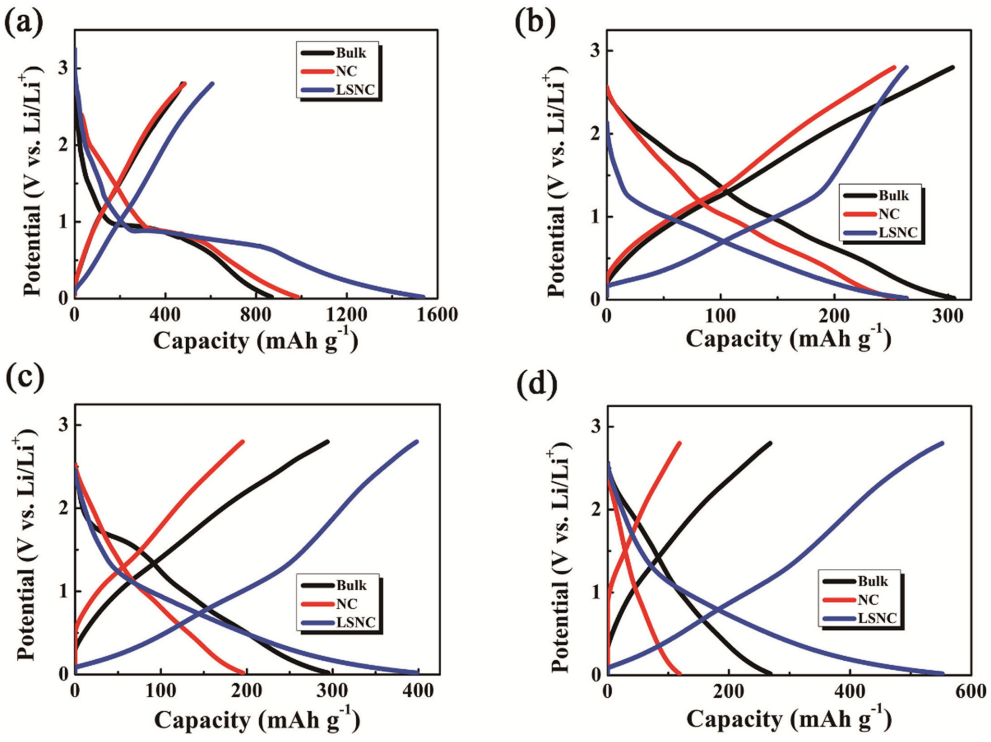

Fig. 2. Galvanostatic charge/discharge profiles of bulk (black), NC (red), LSNC (navy) material. Each profile is results of (a) initial, (b) 50^{th}, (c) 200^{th} and (d) 400^{th} cycle.

486 and 1537/607 mAh g^{-1}, respectively. When compared with the literature about VF_3 material, the high initial discharge capacity of 607 mAh g^{-1} in LSNC anode which is close to theoretical value of 745 mAh g^{-1} is the highest discharge capacity ever reported. This very high capacity reflected that our characteristic nanocrystal structure with churros shape and ligand stripping can be highly helpful for the accommodation of Li^+ and following conversion reaction with VF_3. In the previous literature, our bulk and other nano VF_3 material results [12], the discharge capacity of each material was 440~, 485 and 485 mAh g^{-1}, respectively, which is much lower than our LSNC, indicative of the better accessibility of charge storage sites in our VF_3 material. As shown in Fig. 1a, charge plateau of initial lithiation was shown at ~0.8 V (vs. Li/Li^+) and caused by decomposition of electrolyte and amorphization of conversion-based Li-ion storage materials [17]. Note that this disappearance of the plateau indicates entire amorphization of the electrode material and may be ascribed to its nano-sized nature. [13,17] As one can see in Fig. 1b–d, profiles of bulk material show slight plateau compared to NC and LSNC anodes. Furthermore, note that sloped voltage patterns during charge-discharge are preferable to predicting state of charge (SOC) in LIBs [18,19]. Interestingly, capacity of the LSNC gradually increased and surpassed the other materials as the cycle proceeds.

To elucidate the high-reversible nature and capacity recovery, differential capacity plot against voltage (V vs. Li/Li^+) was presented in Fig. 3. The differential capacity curves were obtained from charge/discharge profiles of the Fig. 2. At the first cycle in Fig. 3a, typical reduction peaks are shown under 0.8 V (vs. Li/Li^+), which is related to the amorphization and decomposition. While no prominent peaks were found as expected, few small and wide peak pairs which are probably attributed to conversion reaction, were found between 0.02–0.5, 1.0–1.5 V (vs. Li/Li^+). The difference of voltage position of peak pair has been associated with voltage hysteresis, which is due to different spatial distribution of M/LiF bicontinuous network determined by reaction kinetics, and this can be controlled and optimized by microstructure designing of a material [24]. The small difference of hysteresis in our LSNC anode, therefore, implied highly optimized structure for reaction kinetics. Note that while the peak

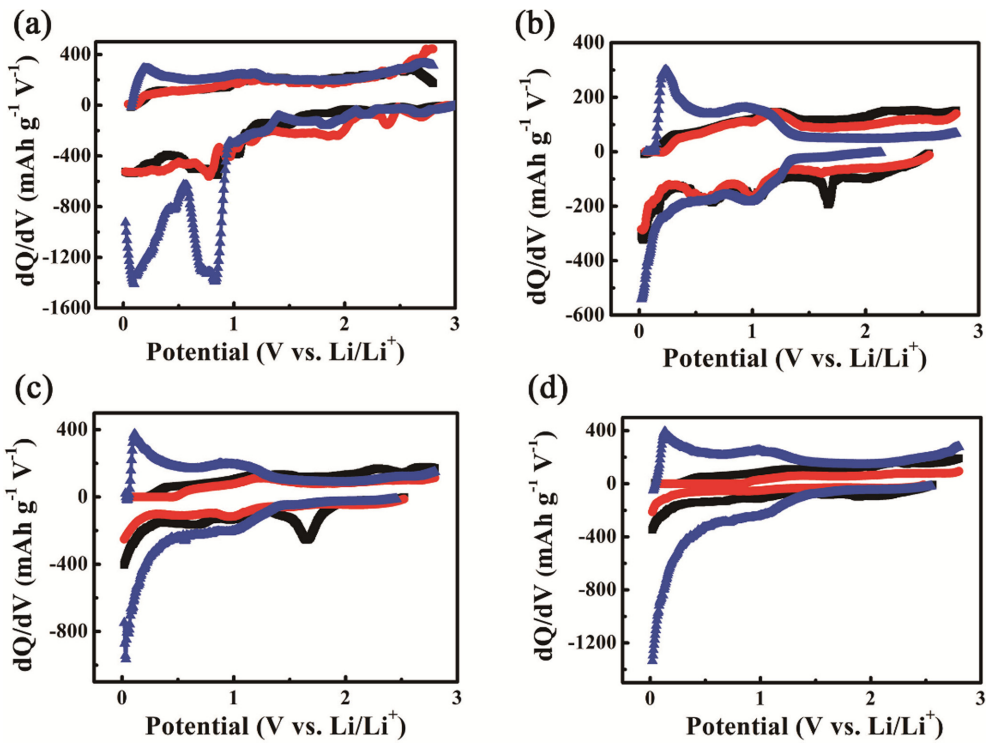

Fig. 3. Differential capacity plotted against potential window (0.02–2.8 V) obtained from the galvanostatic charge/discharge profiles. Each bulk, NC and LSNC's profile is displayed by ■, ●, ▲. The results represent (a) initial, (b) 50^{th}, (c) 200^{th}, and (d) 400^{th} cycle.

pairs of the bulk and NC faded, peak signal of the LSNC gradually increased. As seen in Fig. 3b–d, polarization between charge and discharge voltage decreases as the cycle proceeds and the overall voltage patterns during charge/discharge almost remained similar with an increase of capacity. Note that differential capacity increased under 1.0 V (Li/Li^+) on the charge direction, while similar increase happened under 1.5 V (Li/Li^+) during the discharge direction. It is certain that the capacity increase during cycling in Fig. 2 was attributed to the larger capacity contribution below 1 V during charging, and the increased capacity under 1.5 V during discharging. These typical phenomena are probably related to the slow builds-up of gel-like layer over several cycles because electrolyte penetration to the internal surface of active material is more difficult than to the outer surface. Since VF_3 conversion reaction produced major capacity, it can be assumed that more electrochemically active gel-like layer generated to produce low polarization and enhanced capacity. It is reported that the gel-like layer slowly builds-up over several cycles since electrolyte penetration to the internal surface of active material is more difficult than to the outer surface [26]. These expected phenomena require further investigation using in and ex-situ XRD, TEM and XPS, which is be conducted.

Cycle and rate performance of the individual VF_3 anodes were illustrated in Fig. 4 with C-rate at 0.5 C and from 0.1 to 2 C, respectively. During 500 cycles in Fig. 4a, specific capacity of the LSNC was gradually increased while the other anodes have been faded, which are consistent with the pre-mentioned results. Typically, the LSNC electrode displayed somewhat irreversible Li-ion storage until 10^{th} cycle nature. These are formation cycles widely observed in LIBs [3,17,22,23]. After initial 10 cycles, coulombic efficiency reaches almost 100% indicative of the high-reversible. The efficiency maintained above 98% during afterward cycle test. Then the capacity became gradually decreased till the 49^{th} cycle, and afterward, linear increase of available capacity was observed, which reached to 633 mAh g^{-1} at the 500^{th} cycle which is near to theoretical capacity with maintaining a high cycle efficiency. Note that this phenomenon is typically explained as reversible growth of an amorphous gel-like layer originated from kinetically activated electrolyte and the interfacial lithium storage [25–29]. In Fig. 4b, LSNC showed stable rate performance until 2 C and recovered its capacity when the current of 0.5 C applied again, which indicated that the anode performance of our LSNC is superior than other conversion-based anode materials including the bulk and NC material [20,21]. Note that the rate results of LSNC were obtained after 500 cycles, while the others' obtained after 10 cycles. Despite cycle difference, rate retention of LSNC surpasses the others only except for 2 C.

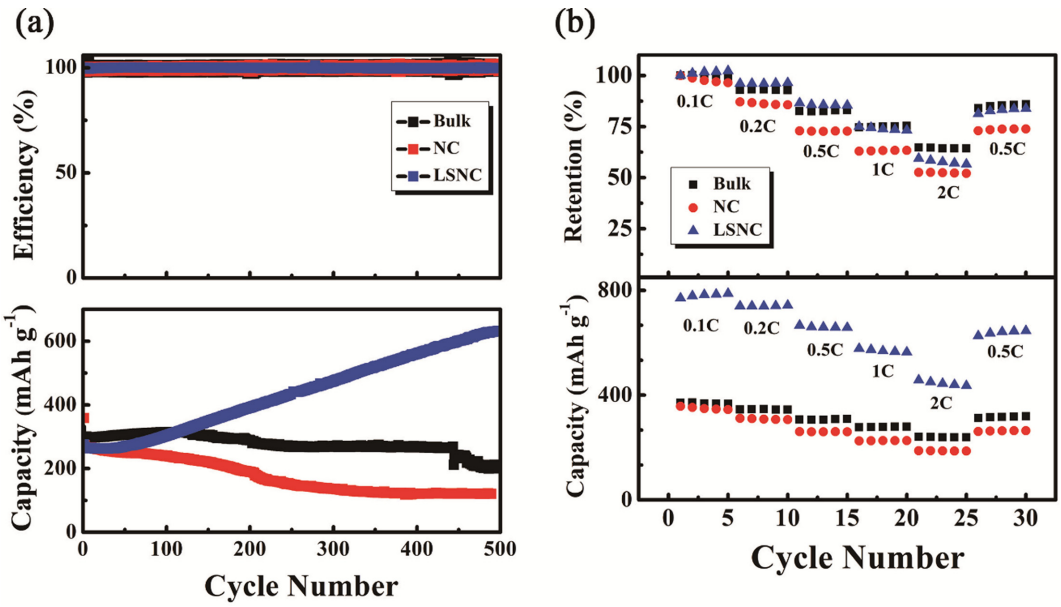

Fig. 4. (a) Cycle performance of bulk (■), NC (●), LSNC (▲) material (0.5C). (b) Rate performance of the materials. Note that results of bulk and NC material were obtained after 10^{th} cycle, while the LSNC's was obtained after 500^{th} cycle.

For further investigation of the reversibility and gradual increase of capacity during cycles, galvanostatic intermittent titration technique (GITT) and was conducted on the electrode. The GITT was applied to study the polarization behavior of the electrode during cycling at 11th and 505th cycle and according profiles were plotted in Fig. 4a. To reach quasi-open-circuit-voltage (QOCV) from closed-circuit-voltage (CCV), the current was interrupted periodically. The polarization was obtained from the difference between the QOCV and CCV. It is widely known that potential difference is contribute to the charge-transfer and ohmic resistance [30]. Fig. 4b shows the variation of the polarization according to QOCV at the 11th and 506th cycle, respectively. During

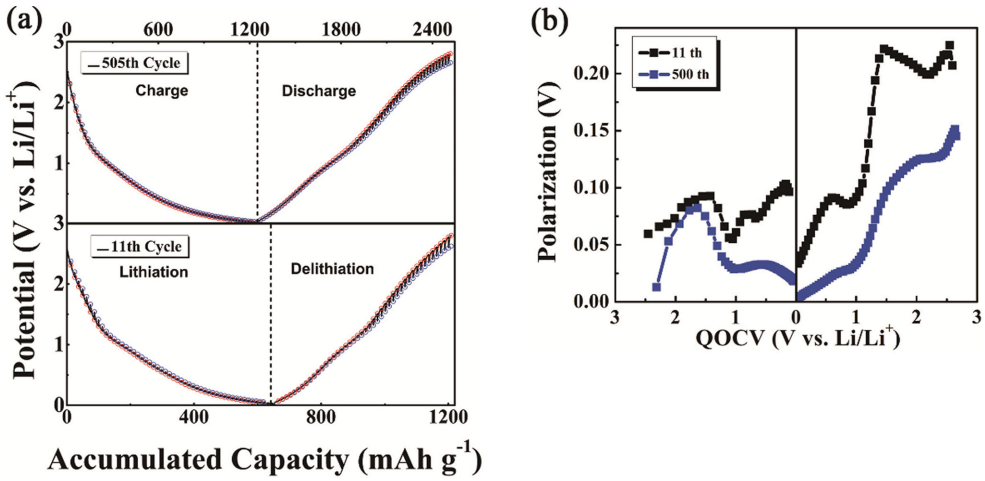

Fig. 5. (a) GITT profiles of 11th and 505th cycle and (b) polarization profiles calculated from the GITT curves.

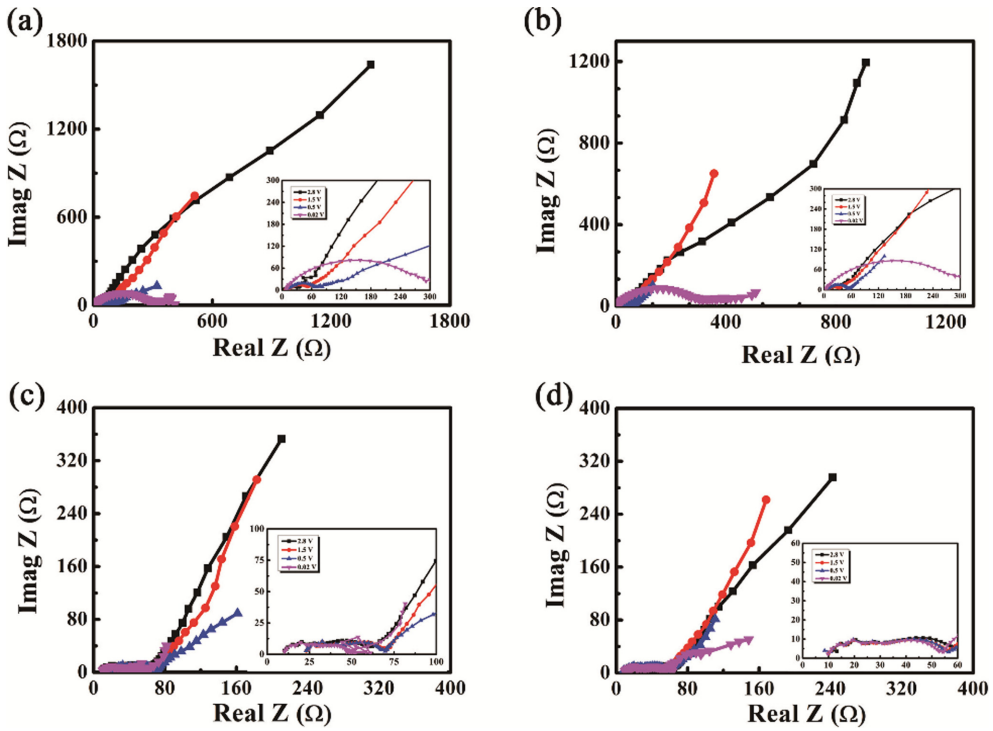

Fig. 6. EIS results of LSNC electrode plotted as Nyquist plot and obtained during (a) 12th charge, (b) 12th discharge, (c) 506th charge and (d) 506th discharge. These are conducted at 2.8 V (■), 1.5 V (●), 0.5 V (▲) and 0.02 V (▼).

charge (lithiation), polarization increased until 1.5 V due to the bond cleavage of metal fluoride during conversion reaction and it sharp decrease was commonly observed under 1.5 V, which is attributed to the formation of the conductive vanadium metal inside the electrode [31,32]. However, after the QOCV became lower than 1.0 V (vs. Li/Li^+), polarization of 11th cycled electrode became larger while a contrast behavior occurred in 505^{th} cycled electrode. On discharge direction (delithiation), both cycle displays similar increasing polarization, which is contributed to the decrease of conductive metallic species and increase of contact resistance due to the delithiation that contracts electrode layer. During the whole discharge process, polarization profiles exhibited lowered values after cycles. Despite each direction of polarization values on 11^{th} cycle mismatched, it should be note that still the reaction potential of 500^{th} cycle shows reversibility. Moreover, the values well-matched after cycles (505^{th} cycle). It seems that the slowly grown active gel-like layer lowered the polarization and enhanced reversibility of charge/discharge process.

The EIS results are displayed as Nyquist plot in Fig. 6 to elaborate charge/discharge phenomena of the LSNC material. The results show reversibility of the material as expected. The semi-circle region in Nyquist plot is associated to the charge-transfer reactions and electrical conduction within the electrode material [33]. Profiles show consistent increase of semi-circle region according to potential decrease which can be ascribed to increase of charge-transfer resistance (R_{CT}) coming from conversion reaction. Remaining tail-like profile is related to inter and inner particle diffusion resistance; Warburg resistance (R_W). It seems that large R_W of 2.8 V contributes to Li^+ diffusion hinderance emerged by SEI film. However, the R_W and overall resistance decreases as the material forms the M/LiF bicontinous gel-like layter matrix after several cycles.

CONCLUSIONS

In summary, we report VF_3 NCs with novel structure prepared by facile colloidal synthesis. The electrochemical performance of the NCs as an anode material in LIBs was evaluated after removal of organic ligands. The results showed much higher capacity and comparable reaction voltage reported elsewhere [12], simultaneously, highly improved features, such as a rate capability, robustness and reversibility, were appeared. Further investigation should be done in the future; however, preferable features are credited to the novel morphology (or structure) which might have affected the bicontinuous M/LiF network, either its interface within each nanoparticle [13].

ACKNOWLEDGEMENTS

This research was supported by the Chung-Ang University Research Scholarship Grants in 2022.

This work was supported by the National Research Foundation of Korea (NRF) grant funded by the Ministry of Science and ICT (MSIT, Korea) (RS-2023-00255695). This work was also supported by the Announcement of New Call for Material Parts Technology Development Program by the Ministry of Trade, Industry and Energy (MOTIE, Korea). (No. 20014562)

REFERENCES

[1] B. Dunn, H. Kamath, and J.-M. Tarascon, Science, 2011, 334, 928.

[2] X. Xin, X. F. Zhou, J. Wu, X. Yao, and Z. Liu, ACS Nano, 2012, 6(12), 11035–11043.

[3] C. He, S. Wu, N. Zhao, C. Shi, E. Liu, and J. Li, ACS Nano, 2013, 7(5), 4459–4469.

[4] J.-M. Tarascon, Phil. Trans. R. Soc. A, 2010, 368, 3227–3241.

[5] L. Xu, C. Kim, A. K. Shukla, A. Dong, T. M. Mattox, D. J. Milliron, and J. Cabana, Nano Lett., 2013, 13(4), 1800–1805.

[6] M. I. Bodnarchuk, K. V. Kravchyk, F. Krumeich, S. Wang, and M. V. Kovalenko, ACS Nano, 2014, 8(3), 2360–2368.

[7] B. Koo, H. Xiong, M. D. Slater, V. B. Prakapenka, M. Balasubramanian, P. Podsiadlo, C. S. Johnson, T. Rajh, and E. V. Shevchenko, Nano Lett., 2012, 12(5), 2429–2435.

[8] X. Xu, R. Cao, S. Jeong, and J. Cho, Nano Lett., 2012, 12(9), 4988–4991.

[9] M. H. Oh, T. Yu, S.-H. Yu, B. Lim, K.-T. Ko, M.-G. Willinger, D.-H. Seo, B. H. Kim, M. G. Cho, J.-H. Park, K. Kang, Y.-E. Sung, N. Pinna, and T. Hyeon, Science, 2013, 340, 964–968.

[10] S. Goriparti, E. Miele, F. De Angelis, E. Di Fabrizio, R. Proietti Zaccaria, and C. Capiglia, J. Power Sources, 2014, 257, 421–443.

[11] N. Nitta, F. Wu, J. T. Lee, and G. Yushin, Mater. Today, 2015, 18(5), 252–264.
[12] H. Li, G. Richter, and J. Maier, Adv. Mater., 2003, 15(9), 736–739.
[13] F. Wang, R. Robert, N. A. Chernova, N. Pereira, F. Omenya, F. Badway, X. Hua, M. Ruotolo, R. Zhang, L. Wu, V. Volkov, D. Su, B. Key, M. S. Whittingham, C. P. Grey, G. G. Amatucci, Y. Zhu, and J. Graetz, J. Am. Chem. Soc., 2011, 133(46), 18828–18836.
[14] E. L. Rosen, R. Buonsanti, A. Llordes, A. M. Sawvel, D. J. Milliron, and B. A. Helms, Angew. Chem. Int. Ed., 2012, 51(3), 684–689.
[15] H. D. Lutz, J. Himmrich, and M. Schmidt, J. Alloys Compd., 1996, 241(1–2), 1–9.
[16] M. F. Oszajca, K. V. Kravchyk, M. Walter, F. Krieg, M. I. Bodnarchuk, and M. V. Kovalenko, Nanoscale, 2015, 7, 16601–16605.
[17] P. Poizot, S. Laruelle, S. Grugeon, L. Dupont, and J.-M. Tarascon, Nature, 2000, 407, 496–499.
[18] Y. Zhou, J. Lee, C. W. Lee, M. Wu, and S. Yoon, ChemSusChem, 2012, 5(12), 2376–2382.
[19] Y. Zhou, Y. Kim, C. Jo, J. Lee, C. W. Lee, and S. Yoon, Chem. Commun., 2011, 47, 4944–4946.
[20] M. Ko, S. Chae, J. Ma, N. Kim, H.-W. Lee, Y. Cui, and J. Cho, Nat. Energy, 2016, 1, 16113.
[21] Y. Wu, L.-Y. Wang, Y.-F. Li, Z.-Y. Zhao, L.-W. Yin, H. Li, and Y.-J. Bai, J. Phys. Chem. C, 2017, 121(24), 13052–13058.
[22] C. Jo, Y. Kim, J. Hwang, J. Shim, J. Chun, and J. Lee, Chem. Mater., 2014, 26(11), 3508–3514.
[23] K. Qian, L. Tang, M. Wagemaker, Y.-B. He, D. Liu, H. Li, R. Shi, B. Li, and F. Kang, Adv. Sci., 2017, 4(11), 1700205.
[24] L. Li, R. Jacobs, P. Gao, L. Gan, F. Wang, D. Morgan, and S. Jin, J. Am. Chem. Soc., 2016, 138(8), 2838–2848.
[25] L. Li, K. H. Seng, Z. Chen, Z. Guo, and H. K. Liu, Nanoscale, 2013, 5, 1922–1928.
[26] L. Hu, H. Zhong, X. R. Zheng, Y. Huang, P. Zhang, and Q. Chen, Sci. Rep., 2012, 2, 986.
[27] W. Wei, S. Yang, H. Zhou, I. Lieberwirth, X. Feng, and K. Müllen, Adv. Mater., 2013, 25(21), 2909–2914.
[28] Z. Bai, Z. Ju, C. Guo, Y. Qian, B. Tang, and S. Xiong, Nanoscale, 2014, 6, 3268–3273.
[29] C. Wang, Y. Zhao, D. Su, C. Ding, L. Wang, D. Yan, J. Li, and H. Jin, Electrochim. Acta, 2017, 231, 272–278.
[30] J. H. Ryu, J. W. Kim, Y.-E. Sung, and S. M. Oh, Electrochem. Solid-state Lett., 2004, 7, A306–A309.
[31] S. Yoon, C. Jo, S. Y. Noh, C. W. Lee, J. H. Song, and J. Lee, Phys. Chem. Chem. Phys., 2011, 13, 11060–11066.
[32] W.-J. Li and Z.-W. Fu, Appl. Surf. Sci., 2010, 256(8), 2447–2452.
[33] Y. Kim, C. Jo, J. Lee, C. W. Lee, and S. Yoon, J. Mater. Chem., 2012, 22, 1453–1458.